Steady-state linear optical properties and Kerr nonlinear optical response of a four-level quantum dot with phonon-assisted transition*

Yan-Chao She(佘彦超)[1,2,†], Ting-Ting Luo(罗婷婷)[2], Wei-Xi Zhang(张蔚曦)[1], Mao-Wu Ran(冉茂武)[1], and Deng-Long Wang(王登龙)[2,‡]

[1] College of Physics and Electronic Engineering, Tongren University, Tongren 554300, China
[2] School of Physics and Optoelectronices, Xiangtan University, Xiangtan 411105, China

(Received 15 May 2015; revised manuscript received 14 August 2015; published online 30 November 2015)

The linear optical properties and Kerr nonlinear optical response in a four-level loop configuration GaAs/AlGaAs semiconductor quantum dot are analytically studied with the phonon-assisted transition (PAT). It is shown that the changes among a single electromagnetically induced transparency (EIT) window, a double EIT window and the amplification of the probe field in the absorption curves can be controlled by varying the strength of PAT κ. Meanwhile, double switching from the anomalous dispersion regime to the normal dispersion regime can likely be achieved by increasing the Rabi energy of the external optical control field. Furthermore, we demonstrate that the group velocity of the probe field can be practically regulated by varying the PAT and the intensity of the optical control field. In the nonlinear case, it is shown that the large SPM and XPM can be achieved as linear absorption vanishes simultaneously, and the PAT can suppress both third-order self-Kerr and the cross-Kerr nonlinear effect of the QD. Our study is much more practical than its atomic counterpart due to its flexible design and the controllable interference strength, and may provide some new possibilities for technological applications.

Keywords: electromagnetically induced transparency, phonon-assisted transition, semiconductor quantum dot

PACS: 42.50.Gy, 78.67.De **DOI:** 10.1088/1674-1056/25/1/014202

1. Introduction

In the past decade, a great deal of attention has been paid to the investigation of quantum optical phenomena based on quantum coherence and interference in semiconductor quantum dot (SQD) and semiconductor quantum dot molecule (SQDM), such as, electromagnetically induced transparency (EIT),[1,2] tunneling-induced transparency (TIT),[3] Autler–Townes (AT) splitting, Mollow absorption spectrum (MAS) splitting,[4] and coherent control of the electron tunneling,[5] owing to their excellent properties such as long dephasing times, and preservation of atomic-like properties (e.g., discrete energy levels) at high temperatures.[6,7] Furthermore, their quantum properties, transition energies, dipole moments, and symmetries can be well manipulated and engineered as desired by choosing the materials and structure dimensions or by applying external fields in device design.[8] It turns out, however, that contrary to their atomic counterparts, QDs have strong temperature-dependent dephasing of the optical polarization.[9] Such a decoherence caused by the interaction of the electrons with the lattice vibrations (phonons) is inevitable in a solid state structure, thus presenting a fundamental obstacle for its applications in quantum computing.[10] Numerous experiments, such as recent measurements of photoluminescence of self-assembled quantum dots, reveal remarkably high probabilities of phonon-assisted transitions (PATs).[11,12] In addition, controllably varied group velocity can make possible the device applications such as all-optical buffers, ultralow group velocity optical modulators, and variable true time delay.[13–16] To design such a device on a semiconductor platform is not only of scientific interest but also essential for future system integration.[17] In addition, both theoretically and experimentally, the giant third-order nonlinear susceptibility with reducing linear absorption has been one of the most extensively studied phenomena, for the third-order Kerr nonlinearity plays an important role in nonlinear optics with applications from optical shutters to the generation of optical solitons.[18–23] Therefore, we here investigate the linear optical properties and Kerr nonlinear optical response of the probe field affected by PAT in a four-level loop configuration InGaAs/GaAs semiconductor quantum dot.

2. Theoretical model

We consider a self-assembled SQD structure which interacts with a weak pulsed probe field p and signal field s

*Project supported by the National Natural Science Foundation of China (Grant No. 61367003), the Scientific Research Fund of Hunan Provincial Education Department, China (Grant No. 12A140), and the Scientific Research Fund of Guizhou Provincial Education Department, China (Grant Nos. KY[2015]384 and KY[2015]446).

†Corresponding author. E-mail: sheyanchao316@163.com
‡Corresponding author. E-mail: dlwang@xtu.edu.cn

© 2016 Chinese Physical Society and IOP Publishing Ltd

and two continuous-wave (cw) control fields (called control-a and control-b) as depicted in Fig. 1. The weak probe field with half the Rabi frequency $\Omega_{\rm p} = (\mu_{01} \cdot e_{\rm p})E_{\rm p}/(2\hbar)$ (with the center frequency $\omega_{\rm p}$ and wavenumber $k_{\rm p} = \omega_{\rm p}/c$) acts on the $|0\rangle \rightarrow |1\rangle$ transition. The signal field with half the Rabi frequency $\Omega_{\rm s} = (\mu_{02} \cdot e_{\rm s})E_{\rm s}/(2\hbar)$ (with the center frequency $\omega_{\rm s}$ and wavenumber $k_{\rm s} = \omega_{\rm s}/c$) acts on the $|0\rangle \rightarrow |2\rangle$ transition. The two strong control fields with half the Rabi frequency $\Omega_a = (\mu_{13} \cdot e_a)E_a/(2\hbar)$ and $\Omega_b = (\mu_{23} \cdot e_b)E_b/(2\hbar)$ (with the center frequencies ω_a and ω_b respectively) act on the $|1\rangle \rightarrow |3\rangle$ and $|2\rangle \rightarrow |3\rangle$transitions, respectively. Here, μ_{ij} $(i, j = 1-4)$ and $e_{\rm p(s,}a, b)$ are the dipole moments of the $|i\rangle \rightarrow |j\rangle$ transitions and the polarization unit vectors of the optical field, respectively. The electric field vector of the system can be written as $E_{\rm p(s,}a,b)$. According to previous reports,[23,24] this structure under consideration consists of GaAs/Al_xGa_{1-x}As component with 15 periods of 17.5-nm GaAs layer and 25-nm $Al_{0.3}Ga_{0.7}$ barriers, grown by molecular beam epitaxy. The GaAs layer samples can be held at 6 K in a helium flow cryostat. The samples are etched to remove the GaAs substrate layer and allow transmission. In Fig. 1, the ground state $|0\rangle$, one-excited states $|1\rangle$ and $|2\rangle$, and biexcition state $|3\rangle$ resemble a four-level loop configuration. It should be noted that states $|1\rangle$ and $|2\rangle$ result from fine-structure splitting of one-exciton state, which can be tuned by many methods in experiment. However, owing to this fine-structure splitting being about tens of μeV, it is necessary to consider the phonon-assisted transition (PAT) between the two exciton states in the process.

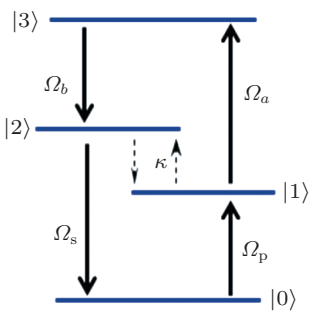


Fig. 1. (color online) Energy-level arrangement of GaAs/AlGaAs QD under study.

By adopting the standard approach,[25] the interaction of the structure with fields can be described by the Schrödinger equation in the interaction picture as

$$\mathrm{i}\frac{\partial|\psi\rangle}{\partial t} = H|\psi\rangle, \tag{1}$$

where the Hamiltonian H reads

$$\begin{aligned} H = {} & \Delta_{\rm p}|1\rangle\langle 1| + (\Delta_{\rm p}+\Delta_a)|3\rangle\langle 3| + (\Delta_{\rm p}+\Delta_a-\Delta_b)|2\rangle\langle 2| \\ & -(\Omega_{\rm p}|1\rangle\langle 0| + \Omega_a|3\rangle\langle 1| + \Omega_b|3\rangle\langle 2| \\ & +\Omega_{\rm s}|2\rangle\langle 0| + \mathrm{i}\kappa|2\rangle\langle 1| + \mathrm{H.c.}), \end{aligned}$$

and κ denotes the strength of PAT, H.c. being the Hermitian conjugate terms, $\Delta_{\rm p} = \omega_{10} - \omega_{\rm p}$, $\Delta_a = \omega_{31} - \omega_a$, and $\Delta_b = \omega_{32} - \omega_b$ being the one-photon detunings denoting the frequency differences between the center frequency and the intersubband transitions ω_{ij} $(i, j = 1$–$4)$ of the levels $|i\rangle \leftrightarrow |j\rangle$, respectively. Under the rotating-wave and electro-dipole approximations, the evolution equations for the slowly varying probability amplitudes A_j of the four levels can be read as

$$\frac{\partial A_0}{\partial t} = \mathrm{i}\Omega_{\rm p}A_1 + \mathrm{i}\Omega_{\rm s}A_2, \tag{2a}$$

$$\frac{\partial A_1}{\partial t} = -d_1A_1 + \mathrm{i}\Omega_{\rm p}A_0 + \mathrm{i}\Omega_aA_3 - \kappa A_2, \tag{2b}$$

$$\frac{\partial A_2}{\partial t} = -d_2A_2 + \mathrm{i}\Omega_{\rm s}A_0 + \mathrm{i}\Omega_bA_3 - \kappa A_1, \tag{2c}$$

$$\frac{\partial A_3}{\partial t} = -d_3A_3 + \mathrm{i}\Omega_aA_1 + \mathrm{i}\Omega_bA_2, \tag{2d}$$

where A_j is the probability of the level $|j\rangle$ $(j = 1-4)$, $d_1 = \mathrm{i}\Delta_{\rm p} + \gamma_1$, $d_2 = \mathrm{i}\Delta_{\rm s} + \gamma_2$, and $d_3 = \mathrm{i}(\Delta_{\rm p} + \Delta_{\rm c}) + \gamma_3$, $\gamma_{1(2,3)} = \gamma_{1(2,3)\rm l} + \gamma_{1(2,3)\rm d}$ depict the corresponding total decay rate of level $|j\rangle$, where $\gamma_{1(2,3)\rm l}$ is the population decay rate of level $|1(2,3)\rangle$ mainly due to longitudinal-optical phonon emission events at low temperature, and $\gamma_{1(2,3)\rm d}$ is the dephasing decay rates of quantum coherence of the $|i\rangle \leftrightarrow |j\rangle$ transitions, determined by electron–electron scattering, phonon scattering processes, and the elastic interface roughness.

In the limit of weak probe field and signal field, almost all electrons will remain in the ground state and we may use the steady state approximation. Under this approximation, we can obtain straightforwardly the solutions of Eq. (2) as follows:

$$A_1 = \mathrm{i}\frac{(\Omega_{\rm p}\Omega_b - \Omega_{\rm s}\Omega_a)(|\Omega_b|^2 + d_2d_3) + d_3\Omega_{\rm s}(d_2\Omega_a - \kappa\Omega_b)}{(d_2\Omega_a - \kappa\Omega_b)(\Omega_a\Omega_b + d_3\kappa) - (\kappa\Omega_a - d_1\Omega_b)(|\Omega_b|^2 + d_2d_3)}A_0 = \mathrm{i}D_1A_0, \tag{3a}$$

$$A_2 = \mathrm{i}\frac{(\Omega_a\Omega_b + d_3\kappa)(\Omega_{\rm s}\Omega_a - \Omega_{\rm p}\Omega_{\rm b}) + d_3\Omega_{\rm s}(d_1\Omega_b - \kappa\Omega_a)}{(\Omega_a\Omega_b + d_3\kappa)(d_2\Omega_a - \kappa\Omega_b) - (\kappa\Omega_a - d_1\Omega_b)(|\Omega_b|^2 + d_2d_3)}A_0 = \mathrm{i}D_2A_0, \tag{3b}$$

$$A_3 = -\frac{\Omega_aD_1 + \Omega_bD_2}{d_3}A_0 = D_3A_0. \tag{3c}$$

Considering the conservation condition $|A_0|^2+|A_1|^2+|A_2|^2+|A_3|^2=1$, we obtain

$$|A_0|=\left[1+|A_1|^2+|A_2|^2+|A_3|^2\right]^{-1/2}. \tag{4}$$

Consequently, the expressions of the electric susceptibilities of the probe and the signal fields are

$$\chi_{\rm p}=\frac{N\mu_{01}}{\varepsilon_0 E_{\rm p}}A_1A_0^*=\chi_{\rm p}^{(1)}+\chi_{\rm p}^{(3,{\rm s})}\left|E_{\rm p}\right|^2+\chi_{\rm p}^{(3,{\rm c})}\left|E_{\rm s}\right|^2+\cdots, \tag{5}$$

$$\chi_{\rm s}=\frac{N\mu_{02}}{\varepsilon_0 E_{\rm s}}A_2A_0^*=\chi_{\rm s}^{(1)}+\chi_{\rm s}^{(3,{\rm s})}\left|E_{\rm s}\right|^2+\chi_{\rm s}^{(3,{\rm c})}\left|E_{\rm p}\right|^2+\cdots, \tag{6}$$

respectively. Here, N and ε_0 are the electron density and dielectric coefficient in a vacuum, respectively; $\chi_{\rm p,s}^{(1)}$, $\chi_{\rm p,s}^{(3,{\rm s})}$, and $\chi_{\rm p,s}^{(3,{\rm c})}$ denote the linear susceptibility, the third-order self-Kerr and the cross-Kerr nonlinear susceptibility of the probe and the signal field, respectively. One can obtain

$$\chi_{\rm p}^{(1)}=\frac{N|\mu_{01}|^2}{2\hbar\varepsilon_0}\frac{{\rm i}(d_2d_3+\Omega_b^2)}{|\Omega_a|^2d_2+|\Omega_b|^2d_1+d_1d_2d_3-2\kappa\Omega_a\Omega_b-\kappa^2d_3}, \tag{7a}$$

$$\chi_{\rm ps}^{(3)}=-{\rm i}\frac{N|\mu_{01}|^4}{8\hbar^3\varepsilon_0}\frac{D_{\rm p}}{|d_3|^2D|D|^2}[(|d_3|^2+\Omega_a^2)D_{\rm p}^2+(|d_3|^2+\Omega_b^2)D_{\rm c}^2-\Omega_a\Omega_b[D_{\rm p}D_{\rm c}^*+D_{\rm p}^*D_{\rm c}]], \tag{7b}$$

$$\begin{aligned}\chi_{\rm pc}^{(3)}=&\,{\rm i}\frac{N|\mu_{01}|^2|\mu_{02}|^2}{8\hbar^3\varepsilon_0}\frac{1}{D|D|^2|d_3|^2}\{-D_{\rm p}[(|d_3|^2+|\Omega_a|^2)|D_{\rm c}|^2+(|d_3|^2+|\Omega_b|^2)|D_{\rm s}|^2-\Omega_a\Omega_b(D_{\rm c}D_{\rm s}^*+D_{\rm c}^*D_{\rm s})]\\&+2D_{\rm c}[-(|d_3|^2+\Omega_a^2)(D_{\rm p}D_{\rm c}^*+D_{\rm p}^*D_{\rm c})-(|d_3|^2+\Omega_b^2)(D_{\rm c}D_{\rm s}^*+D_{\rm c}^*D_{\rm s})+\Omega_a\Omega_{\rm b}[D_{\rm p}D_{\rm s}^*+2D_{\rm c}^2+D_{\rm s}D_{\rm p}^*]\},\end{aligned} \tag{7c}$$

$$\chi_{\rm s}^{(1)}=\frac{N|\mu_{02}|^2}{2\hbar\varepsilon_0}\frac{{\rm i}(d_1d_3+|\Omega_a|^2)}{|\Omega_a|^2d_2+|\Omega_b|^2d_1+d_1d_2d_3-2\kappa\Omega_a\Omega_b-\kappa^2d_3}, \tag{7d}$$

$$\chi_{\rm ss}^{(3)}=-{\rm i}\frac{N|\mu_{02}|^4}{8\hbar^3\varepsilon_0}\frac{D_{\rm s}}{|d_3|^2D|D|^2}[(|d_3|^2+|\Omega_a|^2)D_{\rm c}+(|d_3|^2+|\Omega_b|^2)D_{\rm s}-\Omega_a\Omega_b(D_{\rm c}D_{\rm s}^*+D_{\rm s}D_{\rm c}^*)], \tag{7e}$$

$$\begin{aligned}\chi_{\rm sc}^{(3)}=&\,{\rm i}\frac{N|\mu_{01}|^2|\mu_{02}|^2}{8\hbar^2\varepsilon_0}\frac{1}{D|D|^2|d_3|^2}\{-D_{\rm s}[(|d_3|^2+|\Omega_a|^2)|D_{\rm p}|^2+(|d_3|^2+|\Omega_b|^2)|D_{\rm c}|^2-\Omega_a\Omega_b(D_{\rm p}D_{\rm c}^*+D_{\rm c}D_{\rm p}^*)]\\&+2D_{\rm c}[(-|d_3|^2-|\Omega_a|^2)(D_{\rm p}D_{\rm c}^*+D_{\rm c}D_{\rm p}^*)+(-|d_3|^2-|\Omega_b|^2)(D_{\rm s}D_{\rm c}^*+D_{\rm c}D_{\rm s}^*)+\Omega_a\Omega_b(D_{\rm p}D_{\rm s}^*+D_{\rm s}D_{\rm p}^*+2|D_{\rm c}|^2)]\}.\end{aligned} \tag{7f}$$

3. Steady-state linear absorption–dispersion properties and giant Kerr nonlinearities

We first examine the linear absorption–dispersion properties of the system, which are the major contributors to pulse spreading and attenuation. Considering the control-a being resonant with the transition $\Delta_{\rm c}=0$ and $\Delta_{\rm p}=\Delta_{\rm s}$, equations (7a) and (8a) represent a linear dispersion relation. In fact, the imaginary part ${\rm Im}(\chi_{\rm p,s}^{(1)})$ and the real part ${\rm Re}(\chi_{\rm p,s}^{(1)})$ of this susceptibility characterize the linear absorption coefficient of the probe field and linear refractive index, respectively. According to the definition in Ref. [26], if ${\rm Im}(\chi_{\rm p,s}^{(1)})<0$, the probe (signal) field will be amplified. On the contrary, if ${\rm Im}(\chi_{\rm p,s}^{(1)})>0$, the probe (signal) field will be absorbed. The decrease in ${\rm Re}(\chi_{\rm p,s}^{(1)})$ with detuning corresponds to normal dispersion, while the increase in ${\rm Re}(\chi_{\rm p,s}^{(1)})$ with detuning corresponds to anomalous dispersion. In order to obtain the dependence of the linear dispersion properties, each of the absorption (amplification) and dispersion responses can be regarded as a function of the strength of PAT and the cw control field.

Figure 2 shows the plots of linear absorption (amplification) of the probe field $\Omega_{\rm p}$ versus detuning $\Delta_{\rm p}$ for different values of PAT strength κ and control fields $\Omega_{a,b}$. We here consider the realistic parameters for a typical SQD[27] under coherent laser excitation, such as $N=4\times10^{18}$ cm^{-3}, $\mu_{01}=\mu_{02}=3.34\times10^{-26}$ C·cm, $\Delta_{\rm c}=0$, $\gamma_1=\gamma_2=0.054$ meV, and $\gamma_3=0.108$ meV. From Fig. 2(a), we observe that in the absence of PAT and $\Omega_a=\Omega_b=1.5$ meV, the absorption profile splits into two separate peaks, which is also called the Autler–Townes absorption doublet [i.e., the case of forming the EIT transparency window (TW)]. The suppression of the probe field absorption is caused by the quantum destructive interference effect, which drives the coupling control fields and then renders the population in level $|1\rangle$ into dark states. Similar variation tendencies of linear absorption profiles are observed with larger PAT strength (e.g., $\kappa=0.4$ meV and $\kappa=0.8$ meV). As the PAT coefficient κ increases, the width of the TW becomes narrower and the amplitude of the Autler–Townes absorption doublet decreases gradually. When $\Omega_a=1.5$ meV and $\Omega_b=1.0$ meV, and in the absence of PAT [i.e., $\kappa=0$, see the solid curve in Fig. 2(b)], an absorption valley appears at the central frequency ($\Delta_{\rm p}=0$). This implies that the amplification of the probe field can be achieved in a small range around $\Delta_{\rm p}=0$. When κ increases to 0.4 meV, a small peak at the center of the Autler–Townes absorption doublet appears [see the dashed curve in Fig. 2(b)]. This means that a double EIT is formed. More-

over, with increasing κ (e.g., $\kappa = 0.8$ meV), the central peak decreases to zero and the amplitude of the Autler–Townes absorption doublet decreases continuously [see the doted curve in Fig. 2(b)]. In order to contrast, the absorption curve in the case of $\Omega_a = 1.0$ meV, $\Omega_b = 1.5$ meV is depicted in Fig. 2(c). An approximately symmetrical three-absorption-peak configuration arises and this illustrates that there appears a near-perfect double EIT phenomenon in the absence of PAT and $\Omega_a = 1.0$ meV and $\Omega_b = 1.5$ meV. When κ increases to 0.4 meV, the middle absorption peak becomes a valley and its depth decreases with the increase of the strength of PAT. This illustrates that there appears a transformation between a near-perfect double EIT and amplification phenomenon in the presence of PAT in an appropriate range of the control field. In Fig. 2(c), we should notice that the amplification of the probe field (attributed to the four-wave mixing (FWM) effect caused by the control fields and the signal field) can be suppressed by increasing the strength of PAT, for the large strength of PAT may disrupt the efficient feedback coherent four-wave mixing path. The same concept we demonstrate here can also be applied to a clod atomic system.[28,29] However, the medium studied in our work may be much more practical than in previous studies due to its flexible design and the controllable interference strength and the controlled transition energies, dipoles, and symmetries at will.

We study the effect of PAT on the linear dispersion of the system and show in Fig. 3 the variations of real part $\mathrm{Re}(\chi_{\mathrm{p}}^{(1)})$ of the susceptibility of the probe field with detuning Δ_{p} for different values of PAT strength κ and control field $\Omega_{a,b}$. The parameters used are the same as those in Fig. 2. From Fig. 3(a) it follows that the dispersion curve is in the normal dispersion regime around the resonance point when Ω_a is equal to Ω_b.

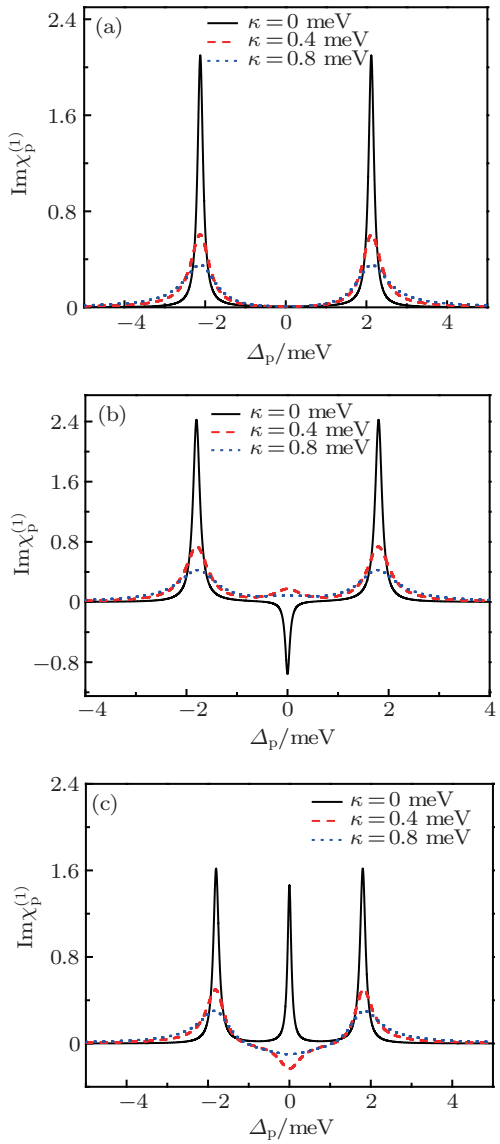


Fig. 2. (color online) Absorption (amplification) spectra of the probe field versus the detuning Δ_{p} with different Rabi energy of the control fields Ω_a and Ω_b: (a) $\Omega_a = \Omega_b = 1.5$ meV, (b) $\Omega_a = 1.0$ meV and $\Omega_b = 1.5$ meV, (c) $\Omega_a = 1.5$ meV and $\Omega_b = 1.0$ meV. Other parameters used are shown in the text.

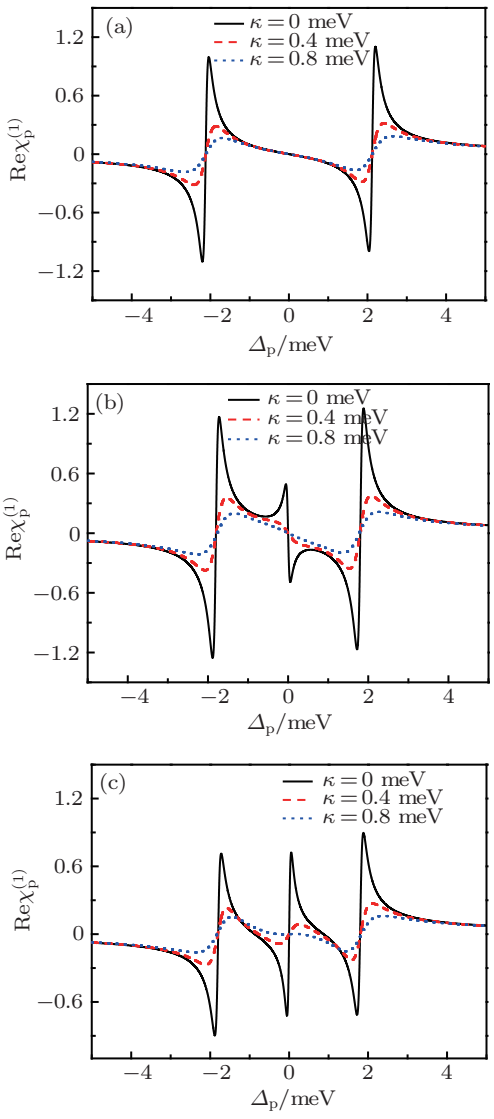


Fig. 3. (color online) Dispersion responses of the probe field versus the detuning Δ_{p} for different Rabi energies of the control fields Ω_a and Ω_b: (a) $\Omega_a = \Omega_b = 1.5$ meV, (b) $\Omega_a = 1.5$ meV and $\Omega_b = 1.0$ meV, (c) $\Omega_a = 1.0$ meV and $\Omega_b = 1.5$ meV. Other parameters used are the same as those in Fig. 2.

The analogous phenomenon appears when $\Omega_a = 1.5$ meV and $\Omega_b = 1.0$ meV as shown in Fig. 3(b). Interestingly, the dispersion curves become more gentle with the increase of the strength of PAT around the resonance point.

This demonstrates that the group velocity of the probe field slows down with the increase of κ. When $\Omega_a = 1.0$ meV and $\Omega_b = 1.5$ meV, the dispersion curve change has changed from a normal dispersion regime to an anomalous dispersion regime and the group velocity of the probe field changes from a positive to a negative value. The result illustrates that it is possible to obtain double switching, in which switching from the normal dispersion regime to the anomalous dispersion regime occurs.

In order to explore the coupling effect of PAT and the external control optical fields on the propagation properties of the probe field, we show in Fig. 4 the variations of group velocity with the strength of the PAT for different values of external control optical field Ω_a.

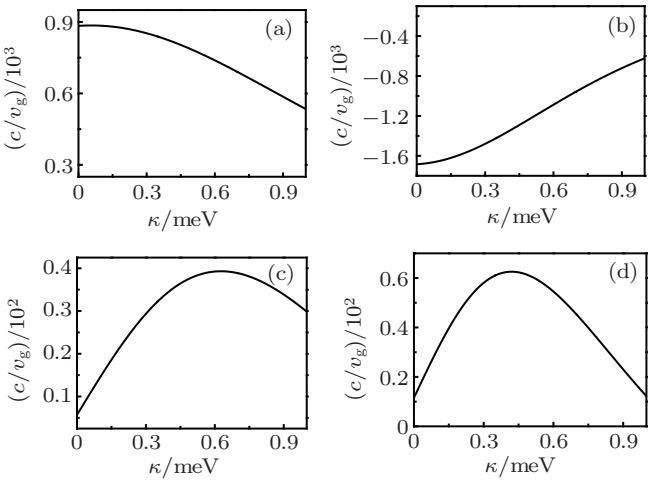


Fig. 4. Variations of group velocity reduction factor of the probe field versus the PAT coefficient κ for different values of Rabi energies of the control fields Ω_a and Ω_b: (a) $\Omega_a = 2.0$ meV and $\Omega_b = 1.5$ meV, (b) $\Omega_a = 1.0$ meV and $\Omega_b = 1.5$ meV, (c) $\Omega_a = \Omega_b = 1.5$ meV, (d) $\Omega_a = \Omega_b = 1.0$ meV. Other parameters used are the same as those in Fig. 2.

As is well known, the group-velocity of a light can be defined as $v_g = c/[n + \omega(\mathrm{d}n/\mathrm{d}\omega)]$ with n being the refractive index of the optical material, and the group velocity reduction factor (GVRF) is defined as $c/v_g = 1 + 2\pi \mathrm{Re}\,\chi\left(\omega_p\right)_{\omega_p=\omega_{10}} + 2\pi\omega_{10}\mathrm{Re}\left(\mathrm{d}\chi/\mathrm{d}\omega_p\right)_{\omega_p=\omega_{10}}$. For the stronger control field Ω_a than Ω_b (e.g., $\Omega_a = 2.0$ meV), one can see from Fig. 4(a) that with κ increasing, the GVRF is nearly inversely proportional to the strength of PAT κ. Under the condition of weak control field Ω_a (e.g., $\Omega_a = 1.0$ meV), the GVRF (group velocity) is negative while it is nearly directly proportional to κ as shown in Fig. 4(b). This occurrence is referred to as "fast light", implying that the peak of a pulse travels in a direction opposite to that of phase velocity and to that of the energy flow.[30] It is because the system is in the anomalous (normal) dispersion and $\partial\,\mathrm{Re}(\chi_p^{(1)})/\partial\Delta_p > 0$ ($\partial\,\mathrm{Re}(\chi_p^{(1)})/\partial\Delta_p < 0$), when $\Omega_a < \Omega_b$ ($\Omega_a > \Omega_b$). The results are qualitative agreement with those in Fig. 3. When Ω_a is equal to Ω_b (e.g., $\Omega_a = \Omega_b = 1.5$ meV) as shown in Fig. 4(c), the GVRF first increases and then decreases, with a maximum factor existing at $\kappa \approx 0.6$ meV. In the case of $\Omega_a = \Omega_b = 1.0$ meV, the maximum factor appears at $\kappa \approx 0.4$ meV, which is smaller than that of $\Omega_a = \Omega_b = 1.5$ meV [see Fig. 4(d)]. From Figs. 4(c) and 4(d), we can conclude that with control field increasing, the maximum GVRF decreases and deviates to the larger side of the PAT κ.

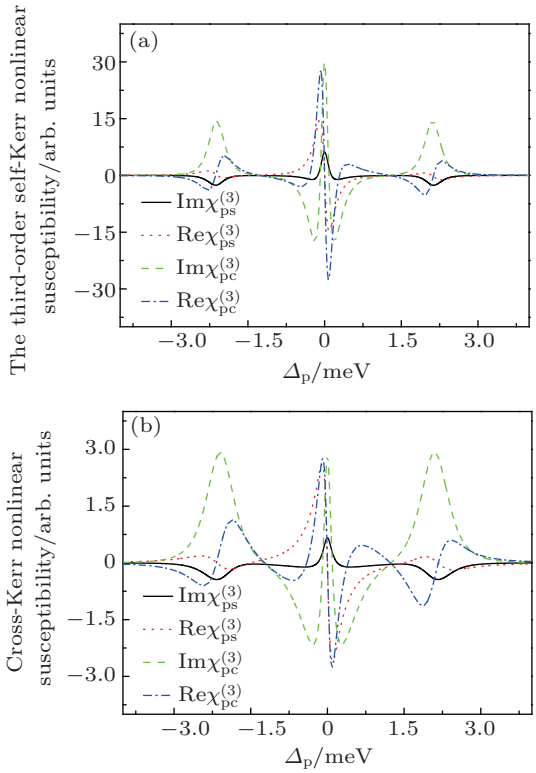


Fig. 5. (color online) Variations of the third-order self-Kerr and the cross-Kerr nonlinear susceptibility of the probe with Δ_p for different strengths of PAT: (a) $\kappa = 0.4$ meV, (b) $\kappa = 0.8$ meV. Other parameters used are the same as those in Fig. 2.

Following the study of the steady-state linear absorption–dispersion properties, one focuses on the Kerr nonlinear in the QD system. In Section 2, we have derived the third-order self-Kerr and the cross-Kerr nonlinear susceptibilities of the probe and the signal field. Moreover, $\chi_{p(s)s}^{(3)}$ and $\chi_{p(s)c}^{(3)}$ are associated with the self-phase modulation (SPM) and cross-phase modulation XPM effects, respectively. Third-order optical nonlinearities described by $\chi^{(3)}$ have been demonstrated both theoretically and experimentally.[31–33] Because of the symmetry of the system, in Fig. 5, we only perform a numerical calculation of the third-order nonlinear susceptibility of the probe field in Eq. (7). The system parameters used are the same as those in Fig. 2(a). From Fig. 5(a), it follows that for a weak PAT strength ($\kappa = 0.4$ meV), nonlinear absorption is weak while the strengths of third-order self-Kerr and the cross-Kerr

nonlinear effect are remarkable in the EIT transparency window as shown in Fig. 2(a). This suggests that the large SPM and XPM can be achieved as linear absorption vanishes simultaneously. This interesting result is produced by coupling the nonlinear susceptibilities associated with XPM and SPM, which is the behavior of a quantum interference between the two different excitation channels: cross-coupling channel and back-coupling channel.[34] In addition, one can readily check that the strengths of third-order self-Kerr and the cross-Kerr nonlinear effect will be suppressed when the strength of the PAT increases to 0.8 meV [see the dotted and dash dotted curves in Fig. 5(b)]. This can be understood as the fact that the strength of PAT is strong so that it can make the back-coupling channel give rise to a destructive interference path way, resulting in the suppressions of XPM and SPM.

4. Conclusions

In this paper, by solving analytically the steady-state Schrödinger equations we demonstrate the optical absorption properties and Kerr nonlinear optical response which can be controlled by the PAT and external optical control field in a loop configuration of a semiconductor QD nanostructure. The results show that in the linear case, when the two external optical control fields are equal, the system exhibits a single TIT window due to the quantum destructive interference effect driven by the control field, and the width of transparency window decreases with PAT strength κ increasing. In particular, the GVRF shows parabolic changes and preserves a maximum value with increasing PAT strength κ, with the control field increasing, the maximum GVRF decreases and deviates to the large side of the PAT strength κ. Interestingly, when $\Omega_a = 1.5$ meV and $\Omega_b = 1.0$ meV, the changes among a single EIT window, a double EIT window and amplifications in the absorption curves can be controlled by varying κ. Meanwhile, the dispersion curves are in normal dispersion regimes. Finally, a near-perfect double EIT appears under the condition of the PAT absenting, however, the amplification of the probe field can be achieved in the presence of PAT when $\Omega_a = 1.0$ meV and $\Omega_b = 1.5$ meV. The dispersion curves are changed to anomalous dispersion regimes around the resonance point, and we show that the group velocity of the probe field becomes negative (the "fast light" may be achieved in our system), when $\Omega_a < \Omega_b$. In the nonlinear case, it is shown that the nonlinear absorption is weak while the strengths of third-order self-Kerr and the cross-Kerr nonlinear effect are remarkable in the EIT transparency window. In other words, the large SPM and XPM can be achieved as linear absorption vanishes simultaneously. In addition, we find that the PAT can suppress both the third-order self-Kerr effect and the cross-Kerr nonlinear effect of the QD. The same concept we demonstrate here can also be applied to a four-level atomic system. However, unlike the cold atomic systems with specific four-level atoms, the conduction subband energy varies with the bias voltage in QD. When we adjust the energy level at different bias voltages, different nonlinear phase shifts can be obtained by such a giant Kerr nonlinearity. Thus our proposed QD structures could be provided as a flexible device to realize voltage-controllable, solid-based phase modulators at low light powers, and a new and effective regulation measure to modulate the optical effect related to quantum coherence and interference can be proposed.

References

[1] Nielsen P K, Thyrrestrup H, Mørk J and Tromborg B 2007 *Opt. Express* **15** 6396
[2] Yuan C H and Zhu K D 2006 *Appl. Phys. Lett.* **89** 052115
[3] Yuan C H, Zhu K D and Jiang Y W 2007 *J. Appl. Phys.* **102** 023109
[4] Villas-Bôas J M, Govorov A O and Ulloa S E 2004 *Phys. Rev. B* **69** 125342
[5] Xu X, Sun B, Berman P R, Steel D G, Bracker A S, Gammon D and Sham L J 2007 *Science* **317** 929
[6] Hang C, Knototop V V and Huang G X 2009 *Phys. Rev. A* **79** 033826
[7] Taranenko V B, Weiss C O and Stolz W 2001 *Opt. Lett.* **26** 1574
[8] Chang-Hasnain C J, Ku P C, Kim J and Chuang S L 2003 *Proc. IEEE* **91** 1884
[9] Devreese J T, Fomin V M, Gladilin V N, Pokatilov E P and Klimin S N 2002 *Nanotechnology* **13** 163
[10] Muljarov E A, Takagahara T and Zimmermann R 2005 *Phys. Rev. Lett.* **95** 177405
[11] Bissiri M, von Högersthal G B H, Bhatti A S, Capizzi M and Frova A 2000 *Phys. Rev. B* **62** 4642
[12] Heitz R, Mukhametzhanov I, Stier O, Madhukar A and Bimberg D 1999 *Phys. Rev. Lett.* **83** 4654
[13] Ku P C, Chang-Hasnain C J and Chuang S L 2002 *Electron. Lett.* **38** 1581
[14] Yanik M F and Fan S 2004 *Phys. Rev. Lett.* **92** 083901
[15] Bao Q, Zhang H, Yang J, Wang S, Tang D Y, Jose R, Ramakrishna S, Lim C T and Loh K P 2010 *Adv. Funct. Mater.* **20** 782
[16] Bao Q, Zhang H, Wang Y, Ni Z, Yan Y, Xiang Z S, Loh K P and Tang D Y 2009 *Adv. Funct. Mater.* **19** 3077
[17] Ku P C, Sedgwick F, Chang-Hasnain C J, Palinginis P, Li T, Wang H, Chang S W and Chuang S L 2004 *Opt. Lett.* **29** 2291
[18] Yan X, Yu Y F and Zhang Z M 2014 *Chin. Phys. B* **23** 060306
[19] Liu W G, Pan F M and Cai L W 2014 *Chin. Phys. B* **23** 064213
[20] Yang X Y and Jiang Y Y 2013 *Chin. Phys. B* **22** 0114204
[21] Bai Y F, Yang W X, Han D A and Yu X Q 2012 *Chin. Phys. B* **21** 0114208
[22] Hao X Y, Zheng A S, Wang Y and Li X G 2012 *Commun. Theor. Phys.* **57** 866
[23] Gammon D, Snow E S, Shanabrook B V, Katzer D S and Park D 1996 *Science* **273** 87
[24] Brunner K, Abstreiter G, Böhm G, Tränkle G and Weimann G 1994 *Phys. Rev. Lett.* **73** 1138
[25] Harris S E 1989 *Phys. Rev. Lett.* **62** 1033
[26] Hao X, Wu J and Wang Y 2012 *J. Opt. Soc. Am. B* **29** 420
[27] Yang W X, Chen A X, Lee R K and Wu Y 2011 *Phys. Rev. A* **84** 013835
[28] Wu Y and Deng L 2004 *Phys. Rev. Lett.* **93** 143904
[29] Au Y J, Fekete D, Pepper D M, Yariv A and Jain R K 1979 *Opt. Lett.* **4** 42
[30] Robert W B 2011 *J. Opt. Soc. Am. B* **28** A38
[31] Sun H, Niu Y, Li R, Jin S and Gong S 2007 *Opt. Lett.* **32** 2475
[32] Hao X, Yang W X, Lü X, Liu J, Huang P, Ding C and Yang X 2008 *Phys. Lett. A* **372** 7081
[33] Hsu P S, Welch G R, Gord J R and Patnaik A K 2011 *Phys. Rev. A* **83** 053819
[34] Yang W X, Zha T T and Lee R K 2009 *Phys. Lett. A* **374** 355